JGR Atmospheres

RESEARCH ARTICLE
10.1029/2022JD037744

CRYOWRF—Model Evaluation and the Effect of Blowing Snow on the Antarctic Surface Mass Balance

Franziska Gerber[1,2], **Varun Sharma**[1,2,3], **and Michael Lehning**[1,2]

[1]WSL Institute for Snow and Avalanche Research SLF, Davos, Switzerland, [2]Laboratory of Cryospheric Sciences, School of Architecture and Civil Engineering, École Polytechnique Fédérale de Lausanne, Lausanne, Switzerland, [3]Sunwell Sàrl, Lausanne, Switzerland

Key Points:

- Evaluation of the coupled Weather Research and Forecasting (WRF) and SNOWPACK model CRYOWRF, including a blowing snow module, shows reasonable representation of blowing snow
- Better representation of atmospheric conditions at a station level by CRYOWRF compared to WRF
- Blowing snow is an important component of the Antarctic surface mass balance, especially in the katabatic regions of the continent

Supporting Information:

Supporting Information may be found in the online version of this article.

Correspondence to:

F. Gerber,
franziska.gerber@slf.ch

Citation:

Gerber, F., Sharma, V., & Lehning, M. (2023). CRYOWRF—Model evaluation and the effect of blowing snow on the Antarctic surface mass balance. *Journal of Geophysical Research: Atmospheres*, *128*, e2022JD037744. https://doi.org/10.1029/2022JD037744

Received 26 AUG 2022
Accepted 13 JUN 2023

Abstract The surface mass balance (SMB) of large polar ice sheets and of snow and ice surfaces in general are incompletely understood because of the complexity of processes involved. One such process, drifting and blowing snow, has only been considered in a very simplified way in current meteorological and climatological models. To address this problem, the CRYOWRF model has been developed, a coupled model between the meteorological Weather Research and Forecasting model (WRF) and the snow model SNOWPACK, augmented by a detailed treatment of drifting and blowing snow. Applying CRYOWRF to the SMB of Antarctica, we find that the model reproduces measurements of SMB with similar errors than current models. Drifting and blowing snow and its sublimation play a particularly important role, especially in regions of strong katabatic winds. The CRYOWRF simulations are also in line with satellite estimates of blowing snow frequency. There is a need to further consolidate results by simulations with a higher grid resolution and by including more measurements of SMB contributions from snow fall to transport and sublimation.

Plain Language Summary Assessing current and predicting future sea level rise in connection with the general fate of our snow and ice masses on Earth requires understanding snow precipitation in extreme environments and the dynamics of snow on the surface. Over large parts of Antarctica, drifting and blowing snow and sublimation, which is the phase change of ice back to atmospheric vapor, are the only surface ablation processes and need therefore to be well quantified. With a new model, that shows similar performance to other models, we find that drifting and blowing snow and its sublimation play an important role for the snow mass balance especially in regions with strong winds. This has consequences not only for the snow mass balance alone but for the whole ice sheet dynamics as well as for estimating precipitation in these extreme environments.

1. Introduction

While ice melt and subsequent runoff on the Antarctic ice sheet (AIS) is increasing due to climate change, snow accumulation may be increasing as well, albeit with significant temporal and spatial heterogeneity (Smith et al., 2020). However, quantitatively the increase in snow accumulation is not understood. Furthermore, large uncertainties in both assessment and future predictions of surface mass balance (SMB) of the AIS and thus, sea level rise, arise from the contribution of drifting and blowing snow (e.g., Gossart et al., 2020).

The effect of drifting and blowing snow (i.e., snow that is lifted from the surface to heights below or above ∼1.8 m, respectively), is widely debated and a large range of values has been presented. One important effect of drifting and blowing snow is its sublimation, which results in a decrease of the SMB. Drifting and blowing snow sublimation over the AIS is estimated to locally reach up to about 85% of annual precipitation based on a simple linear function between ablation and local firn temperatures (Frezzotti et al., 2004). A recent simulation with the Regional Atmospheric and Climate Model (RACMO2), a regional numeric weather prediction model, suggests that drifting and blowing snow sublimation amounts to only 102 Gt y^{-1} (van Wessem et al., 2018), which is 43% less than suggested by a previous version of the model (van Wessem et al., 2018). The regional numerical weather model Modèle Atmosphéric Régional (MAR), shows good agreement with drifting snow measurements in Adélie land (Amory et al., 2021). The study does not provide continent-wide estimates of drifting and blowing snow sublimation. As in Agosta et al. (2019) MAR was applied without activating the drifting and blowing snow module, there are no continental estimates of drifting and blowing snow sublimation available. Estimates based

on satellite data on the other hand are considerably higher for blowing snow sublimation (393 ± 196 Gt y^{-1}) from deep blowing snow layers (Palm et al., 2017).

In-situ measurements of drifting and blowing snow are still scarce due to the remoteness and the harsh environment of Antarctica and they are not fully representative due to the high spatial variability of the process. Remote sensing data of drifting and blowing snow suffers from the fact that information is only available for periods with no or low cloud cover (Palm et al., 2017). Meteorological models with adaptations to Antarctic conditions were applied for large scale modeling of Antarctica including drifting and blowing snow parameterizations such as for example, RACMO (Lenaerts et al., 2012; van den Broeke et al., 2002) and MAR (Amory et al., 2021; Gallée et al., 2013). Blowing snow parameterization (referring to all drifting and blowing snow processes in the models hereafter) in these models, however, relies on simplified process representation, particularly with regards to the parametrization of lower boundary conditions for blowing snow particles. For example, in MAR, blowing snow particles are added to the "precipitation snow" class of the microphysics scheme (which itself is a single-moment bulk scheme). This results in a mixture of precipitation snow and blowing snow that is difficult to disentangle. While RACMO has a double-moment blowing snow scheme as a separate class of particles, it utilizes a single-column representation with no horizontal advection of blowing snow particles. The simplifications in both models can be traced back to the fact that the model resolutions in these codes is limited by the hydrostatic nature of their atmospheric modeling core to remain at a minimum of 5 km. Thus, while these models provide good results at large-scales, they are unable to simulate small-scale phenomena particularly on steeply sloped ice sheets which are common on the continental edges in Antarctica. Finally, RACMO and MAR use simplified parametrizations for the threshold friction velocity ($u_{*,t}$), one of the most important variables for accurately simulating blowing snow. These parametrizations are based on density and age of the top snow layer. There are models available that instead link $u_{*,t}$ directly to snow microstructure (e.g., Lehning et al., 2000; Melo et al., 2022). The recently developed version of WRF, called CRYOWRF (Sharma et al., 2023) allows for a more physical representation of snow transport and blowing snow sublimation. In CRYOWRF, blowing snow is treated online in a non-hydrostatic atmospheric model, allowing to investigate the full chain of interactions between blowing snow and the atmosphere at scales ranging from mesoscale to the turbulent scales. Additionally, the model is capable of running nested simulations, allowing to downscale simulations to high resolution and investigate the effect of horizontal model resolution on the process representation. In CRYOWRF blowing snow is treated in a double moment scheme with 3D advection and turbulent mixing. Between the surface and the first model level of WRF, a finer mesh allows for a higher resolution of the strong gradient of blowing snow close to the surface. The lower boundary conditions for the saltation layer in CRYOWRF are directly dependent on the surface snow microstructure. Finally, the parameterization of the terminal mass and number average fall velocity is based on the latest advances in the cloud microphysics community (Jensen et al., 2017). More details about the model are given in Section 2.1 and Sharma et al. (2023).

In this study we present a first CRYOWRF simulation over the AIS, highlighting its performance and ability to represent the SMB and blowing snow at a coarse resolution on the continental scale. In Section 2 we present CRYOWRF and its peculiarities as well as measurement data used for the evaluation. The general performance of CRYOWRF in representing the atmospheric conditions is shown in Section 3.1. Comparing modeled blowing snow and in-situ measurements we demonstrate a snapshot of the model's ability to represent blowing snow fluxes (Section 3.2). Based on a 10-year simulation we present the SMB and its components (Section 3.3) and estimate the effect of blowing snow on the regional SMB (Section 3.4). The conclusion and outlook (Section 4) summarize our findings and discuss remaining deficiencies of the model and required analysis.

2. Data and Methods

2.1. WRF and CRYOWRF

Simulations are performed with the non-hydrostatic, fully compressible Weather Research and Forecasting (WRF) model version 4.2 (Skamarock et al., 2019) and the recently implemented CRYOWRF v1.0 (Sharma et al., 2023), which couples WRF version 4.2 to the snow model SNOWPACK (Lehning et al., 1999) as a land surface model. In CRYOWRF, blowing snow processes are represented near the surface on a high resolution vertical grid between the surface and the first model level of WRF (Sharma et al., 2023).

Both simulations are run for 10 years and 2 months of spin-off time (1 July 2010–1 September 2020) over the Antarctic continent with a horizontal grid resolution of 27 km and 64 vertical levels up to 100 hPa. Two month of

spin-off time are simulated to allow the uppermost layers of the snow cover to adapt to model physics. The simulations are run for 10 years to remove parts of the interannual variability. Although 10 years are not enough for a climatological study, it corresponds well to the available station observations (Section 3.1). The simulation timestep is 90 s. CRYOWRF includes 8 additional atmospheric levels to resolve blowing snow between the surface and the first model level at approximately 6 to 7 m above ground. In the WRF simulation, called WRF hereafter, the land surface is parameterized using the Noah land-surface model with multi-parameterization options (Noah-MP, Niu et al., 2011; Yang et al., 2011). The CRYOWRF simulation uses SNOWPACK as land-surface model over continental land grid cells, while Noah-MP is active over sea ice. Ice shelves are simulated in the same way as snowpacks on "land." This treatment is similar for SNOWPACK and Noah-MP. Effectively, this means that the lower boundary condition of the ice shelves is not ocean but instead an isothermal "land" layer. This approximation can cause errors only at the final 100–1 km of the iceshelves. In WRF terminology, ice shelves are classified as "LAND" grid points by both SNOWPACK and Noah-MP. SNOWPACK runs with a timestep of 15 min, using the Holtslag surface layer model by Holtslag and De Bruin (1988), the albedo parameterization is based on the albedo parameterization developed by Munneke et al. (2011) and implemented in SNOWPACK by Steger et al. (2017). The water transport in the snowpack is described by a bucket model, commonly used in hydrology. In this approach, water is moved from the upper layer to the layer below only upon saturation. The fine-scale temporal dynamics of this transport are implicitly neglected and the transport is assumed to complete every time-step. Apart from approximating the temporal dynamics, however, this approach has been shown to capture phenomena such as re-freezing, but not ice-lens formation (Wever et al., 2016) and sub-surface ponding amongst others. Additionally, the albedo model described above is able to take into account ponding and re-freezing at the surface. Finally, as the blowing snow scheme is linked directly to the surface micro-structure, the melt-refreeze-blowing snow feedback is simulated as well. The snowpack layer thickness, snow temperature, snow density, grain radius and volume fraction of ice are initialized by the firn densification model (FDM, Ligtenberg et al., 2011) output (forced by RACMO, van Wessem et al., 2018) from the 1 July 2010. The grain bond radius is set to 0.2 times grain radius, the dendricity is set to 0 and the sphericity to 1, indicating rounded snow grains at initial conditions, throughout the snowpack. The blowing snow parameterization near the surface is based on Vionnet et al. (2014) and described in detail in Sharma et al. (2023) and Section 2.1.1. The surface properties of the snowpack are directly linked to blowing snow via the parametrization of the threshold friction velocity. The threshold friction velocity $u_{*,t}$ (m s^{-1}) is computed following (Lehning et al., 2000) and (Schmidt, 1980) as,

$$u_{*,t} = \sqrt{\frac{A_t \rho_{ice} g r_g (SP + 1) + B_t \sigma_{ref} \frac{N_3 r_b^2}{r_g^2}}{\rho_{air}}}, \quad (1)$$

where A_t and B_t are geometrical parameters, SP is the sphericity of the snow grains that varies between 0 and 1, N_3 is the coordination number of the snow grains and σ_{ref} (Pa) is the reference shear strength (which is fixed at 300 Pa). ρ_{ice} (kg m^{-3}) and ρ_{air} (kg m^{-3}) are the ice and air density, respectively. r_g (m) and r_b (m) are the grain radius and bond size between grains, respectively, and g is the gravitational constant (m s^{-2}). Whenever the surface friction velocity is greater than $u_{*,t}$ (m s^{-1}), snow grains begin to saltate over the surface.

Currently, the effect of blowing snow is not accounted for in the radiative scheme of CRYOWRF. The effect has been shown to be able to affect the surface energy balance but also cloud radiative effects (e.g., Hofer et al., 2021). To account for possible effects, the effect of blowing snow on radiation is planned to be implemented in CRYOWRF in future releases. The blowing snow parameterization, unlike SNOWPACK, is called at every WRF timestep to resolve the high temporal variability of the process.

Except for the land surface parameterization, both simulations use the same setup. The planetary boundary layer (PBL) is parameterized by the Mellor-Yamada-Nakanishi-Niino 2.5 level turbulent kinetic energy (MYNN) scheme (Nakanishi & Niino, 2006, 2009), using the scalar mixing option. For the sub-grid-scale turbulence the horizontal Smagorinsky first order closure is used. Microphysics are parameterized using the 2-moment Morrison scheme (Morrison et al., 2005, 2009), which has recently been adapted to polar atmospheric conditions (Vignon et al., 2021). In CRYOWRF blowing snow is represented by a classic double moment hydrometeor model that includes sublimation and deposition along with advection and turbulent diffusion of blowing snow particles throughout the atmosphere (Sharma et al., 2023).

The simulations are initialized and forced by ERA5 reanalysis data (Hersbach et al., 2018a, 2018b). Atmospheric nudging against ERA5 is applied to the upper atmosphere (top 20 atmospheric layers) for zonal and meridional winds. Topography is based on the Reference Elevation Model of Antarctica (REMA) topography (Howat et al., 2019), which has an improved representation of coastal snow free terrain compared to BedMap2 (Fretwell et al., 2013). The landuse categories are based on the AntarcticaLC2000 landuse data set (Hui et al., 2017). REMA and AntarcticaLC2000 static input data for WRF are available from Gerber and Lehning (2020). In the current setup grid cells with a landuse category bare rock are not treated differently from grid cells with a snow/ice cover. However, this option is planned to be investigated in the future.

2.1.1. Blowing Snow in CRYOWRF

Blowing snow in CRYOWRF is implemented following the blowing snow scheme in Meso-NH (Vionnet et al., 2014). As drifting and blowing snow shows the strongest gradient in the first meters above the surface, eight extra layers are added between the surface and the first model level in WRF with the first level at 0.5 m above ground and the 8th level 3 m below the first WRF model layer (Sharma et al., 2023). The layers inbetween are regularly spaced.

To analyze modeled blowing snow compared to the 2G-FlowCapt^{TM} measurements (see Section 2.3) blowing snow flux (QS, kg m^{-2} s^{-1}) from the first n model levels has been integrated over the first 2 m above ground as,

$$QS = \frac{\left(h_1 + \frac{(h_2 - h_1)}{2}\right)}{h_{unit}} * QS_1 + \sum_{i=2}^{n} \frac{\left(\frac{(h_i - h_{i-1}) + (h_{i+1} - h_i)}{2}\right)}{h_{unit}} * QS_i + \frac{\left(\frac{(h_n - h_{n-1}) + (h_{ref} - h_n)}{2}\right)}{h_{unit}} * QS_n, \quad (2)$$

where h_i (m) is the elevation of the ith model level above ground, QS_i (kg m^{-2} s^{-1}) the blowing snow mass flux of the ith level and h_{ref} (m) the reference elevation, up to which the blowing snow mass flux is integrated (i.e., 2 m in our study). n is the first level greater or equal h_{ref} (m). $h_{unit} = 1$ m to keep a unit of kg m^{-2} s^{-1}.

For the comparison to data of the snow particle counter (SPC) at Princess Elizabeth (PE) station (see Section 2.3), the blowing snow mass flux at the lowest model level (i.e., 0.5 m ag) is used for comparison, given that the SPC was installed at ∼50 cm above ground and got closer to the ground due to snow accumulation in the course of time.

2.1.2. Blowing Snow Filtering for Qualitative Comparison to Satellite Data

Blowing snow frequency is based on the blowing snow mixing ratio. Blowing snow mixing ratio of grid cells without blowing snow is, for computational reasons, 10^{-12} kg kg^{-1}. For blowing snow to be detected, a daily mean mixing ratio of at least 10^{-7} kg kg^{-1} day^{-1} is assumed. When limiting blowing snow to 10^{-10} kg kg^{-1} regions with artificial blowing snow patterns are removed. However, blowing snow mixing ratios on $\mathcal{O}(10^{-10}$ kg kg$^{-1})$ correspond to blowing snow amounts that are likely not recognized by either satellites or eye. A recent study for Northern America shows, that blowing snow ratios $<10^{-6}$ kg kg^{-1} do not have an impact on visibility (Letcher et al., 2021). Hence, a blowing snow mixing ratio of 10^{-7} kg kg^{-1} day^{-1} has been assumed, which further results in a reasonable blowing snow extend off continent, given that in CRYOWRF no snow is eroded over sea ice but only deposited. Maps with blowing snow frequencies based on mixing ratio thresholds of 10^{-6} and 10^{-8} kg kg^{-1} day^{-1} are shown in the Supporting Information (Figure S2–S5 in Supporting Information S1) and are discussed in Section 3.2.2.

Blowing snow frequency between 2006 and 2017 has been investigated by Palm et al. (2018) from satellite data of the Cloud-Aerosol Lidar with Orthogonal Polarization (CALIOP) Lidar, which was onboard the Cloud-Aerosol Lidar and Infrared Pathfinder Satellite Observation (CALIPSO) satellite (Winker et al., 2009). To get a measure comparable to the results by Palm et al. (2018) a filter is applied to CRYOWRF results to remove blowing snow that would not be detected by the satellite. Blowing snow in Palm et al. (2018) is detected whenever there is a near-ground signal, which is inline with a cloud optical thickness lower than three. Additionally, only blowing snow layers with a thickness of at least 30 m are detected by the satellite due to the vertical resolution of the measurements. Palm et al. (2018) state that these constraints mainly affect the coastal regions, while over the central continent clouds with an optical thickness of three or more are unusual. Hence, the fraction of potentially missed blowing snow events ranges from around 50% over coastal regions to 5% over central Antarctica. Furthermore, the satellite cannot see anything to the south of 82°S.

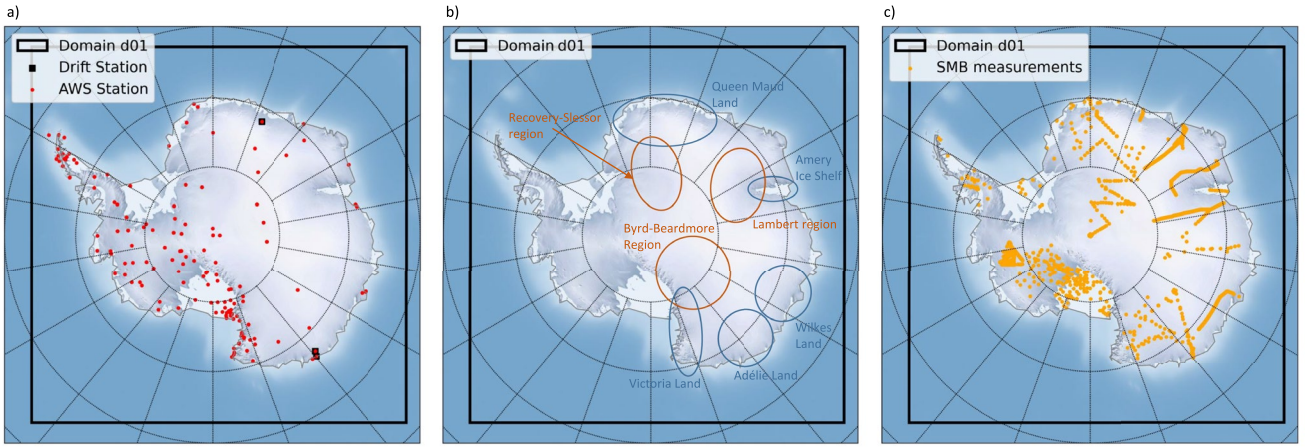

Figure 1. (a) Antarctic atmospheric weather stations (AWS) used for model evaluation (red). Stations with drifting snow measurements are additionally marked by a black square. Not all stations are used for all variables. Details are given in Table S1. Stations apparently off continent are located on islands off continent in the North of the Antarctic Peninsula. The black box marks the simulation domain. The different shades of blue are only for visualization purposes and represent the terrain and highlight the ice shelves. (b) Regions of high blowing snow frequency, matching regions in Scambos et al. (2012) (orange) and regions of lower blowing snow frequencies for comparison to Palm et al. (2018) (blue). (c) Locations of surface mass balance stake measurements.

For the qualitative comparison of CRYOWRF to the results by Palm et al. (2018) based on the satellite blowing snow product (Section 3.2.2), we apply a correction removing the cloudiest days (highest cloud fraction summed over all levels) based on cloudiness levels determined by linearly interpolating the decrease of data availability based on the terrain elevation. This is a very rough approximation compared to the satellite product. For East Antarctica the assumption holds rather well, while the reduction is too weak for West Antarctica and the Antarctic Peninsula (see Figure 2 in Palm et al., 2018). Additionally, blowing snow is detected from the lowest level above 30 m above ground for each grid cell, which is level three or four in our simulation setup depending on the location. Overall, CRYOWRF shows higher than expected amounts of clouds over the central part of Antarctica (not shown). However, the analysis as performed is not affected by the total amount of clouds as the reduction of blowing snow frequency is based on a percentage of the cloudiest days, which is determined by the terrain elevation.

2.2. Atmospheric Weather Stations

A set of 148 atmospheric weather stations (AWS) over the Antarctic continent has been collected from different databases (Antarctic Meteorological Research Center, AMRC; Australian Antarctic Division, AAD; Antarctic Meteo-Climatological Observatory by the Italian National Programme of Antarctic Research, CLIMANTARTIDE; National Oceanic and Atmospheric Administration, NOAA; World Data Center PANGAEA; Japan Meteorological Agency, JMA; Princess Elisabeth, PE; Stations D-17 and D-47 in a transect between Dumont d'Urville and Dome C; Institute for Marine and Atmospheric Research Utrecht, IMAU; British Antarctic Survey, BAS; links and references are given in the Data Availability Statement section). The different weather stations are equipped with different sensors, most of them collecting pressure (125 stations), temperature (137 stations), wind speed and direction (140 stations) and relative humidity (71 stations) data among other quantities. The output frequency of each data set is either 30 min, 1 or 3 hr. Potential temperature (θ) is calculated based on the measured surface pressure (if available). Alternatively, the surface pressure from the model is used for the calculation of θ. Therefore, no additional elevation correction between the actual altitude and the modeled altitude is taken into account. RH is measured with respect to water as far as the authors know. Timeseries of each station were visually inspected and stations with trends or other inconsistencies have been removed. Furthermore, obvious outliers were deleted from the data set. However, other issues like frozen anemometers or malfunctioning sensors may not have been detected.

The set of stations used for the evaluation is based on their measurement period and their availability on the given databases (Figure 1, Table S1). A rough classification about the station locations (coastal, shelf, inland, island) is given in Table S1. Not all stations cover the full 10-year period as simulated by WRF and CRYOWRF. All stations cover at least one full year or consist of non-continuous data of several years (stations not covering the required period are not taken into account and are not listed in Table S1).

WRF and CRYOWRF output surface pressure, 2-m potential temperature (based on the diagnostic 2-m temperature in the model), 10-m wind speed logarithmically corrected to sensor height (if known) otherwise to a sensor height of 5 m has been assumed, given that most Antarctic AWS do not consist of a 10 m tower and the diagnostic 2-m relative humidity (with respect to water) at the closest grid cell to the station (on land) are selected for comparison. To test the significance of the statistics a Mann-Withney-U test was performed on the data with a significance level of 5%.

2.3. Drifting and Blowing Snow Measurements

Measuring drifting and blowing snow is challenging, especially in the remote and harsh environment of Antarctica. In-situ as well as remote sensing techniques have been developed. Satellite data have the advantage to cover larger areas and estimates of spatial variability and frequency of blowing snow occurrence can be achieved (Palm et al., 2017, 2018). However, they are strongly limited to mainly cloud free conditions or conditions with a thin cloud cover (Palm et al., 2017, 2018), while blowing snow often occurs during stormy and overcast periods (Gossart et al., 2017).

Point measurements on the other hand are very limited in space. Both SPCs (Niigata Electric, Japan) and FlowCapt sensors (Amory, 2020) were used in Antarctica. More recently ceilometer data was analyzed to detect drifting and blowing snow (Gossart et al., 2017; Loeb & Kennedy, 2021). However, long time series of continuous measurements are still scarce.

Two multi-year timeseries of drifting snow measurements were collected at the two stations D-17 and D-47 (Figure 1, Table S2 in Supporting Information S1) in a transect between Dumont d'Urville station and Dome C in Adélie land using 2G-FlowCapt^{TM} sensors (Amory, 2020). The two 2G-FlowCapt^{TM} at D-47 were operative between January 2010 and mid 2012. At D-17 a continuous measurement campaign started in December 2012 and is still ongoing. The sensors measure at a frequency of 30 min. At both stations, drifting snow is measured together with wind speed, temperature and relative humidity.

Drifting snow data for D-17 and D-47 is processed as in Amory (2020) and the snow mass flux (η_{DR}, kg m^{-2} s^{-1}) integrated over the first 2 m above ground (h_{ref}) is presented, calculated as

$$\eta_{DR} = \begin{cases} \eta_1 + \eta_2 & h_1 + h_2 \geq h_{ref} \\ (\eta_1 + \eta_2) * \dfrac{h_{ref}}{(h_1 + h_2)} & h_1 + h_2 < h_{ref} \end{cases} \quad (3)$$

where η_1 and η_2 are the snow mass fluxes (in kg m^{-2} s^{-1}) integrated over h_1 (m) and h_2 (m), the exposed parts of the two 2G-FlowCapt^{TM} sensors in meters, respectively. Note: brackets in the formula in Amory (2020) are incorrect (confirmed by C. Amory, corresponding author of Amory, 2020). Timesteps for which drifting snow has been measured but wind speed was 0 m s^{-1} were removed from the data set. Measurements of the lower 2G-FlowCapt^{TM} are not taken into account if it is buried by more than 90 cm.

Additionally, drifting snow measurements from a SPC at PE station, which was installed in December 2016 and measured reliably until June 2017, are used. Unfortunately, no data was recorded afterward due to unknown reasons and the temperature sensor of the SPC failed in the following year. SPC data is recorded with a frequency of 1 s. A correction to the drifting snow measurements is applied based on temperature measured by the internal sensor (Sigmund et al., 2022). For the analysis we calculate hourly mean values.

For both 2G-FlowCapt^{TM} and SPC measurements the comparison to CRYOWRF output only includes times for which measured drifting snow fluxes are available.

2.4. SMB Analysis

To put SMB values from CRYOWRF into context, they are compared to stake SMB measurements from 9,660 locations over the whole continent, using the data set by Agosta et al. (2019), which is based on the data collection detailed in Favier et al. (2013) and Wang et al. (2016) originating from the data set by Vaughan et al. (1999), which is based on averages of SMB over more than 3 years. Furthermore, the data set was augmented with accumulation data by Medley et al. (2014), representing average values between 1985 and 2009. Overall, measurements

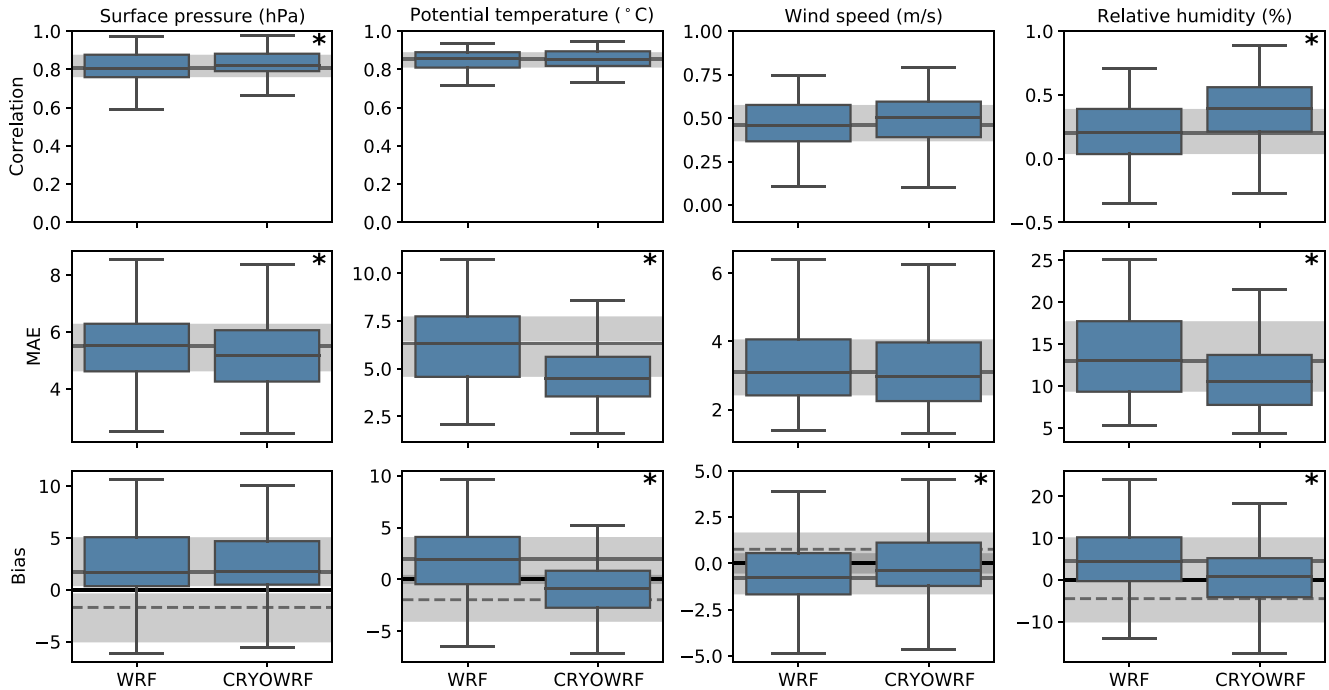

Figure 2. Boxplots of correlation, mean absolute error (MAE) and bias for surface pressure, potential temperature, wind speed and relative humidity for the two model simulation runs WRF and CRYOWRF. The median and 25th- and 75th-quartiles are marked by a gray horizontal line and shaded area, respectively. For the bias the zero line is given in black. Significant differences based on a Mann-Whitney-U test with a significance level of 0.05 are marked with a * on the top right of the panel.

between 1950 and 2015 are included in the analysis. Details about the data set are given in the respective publications and in Agosta et al. (2019). The data was processed by the scripts provided by Agosta (2019). SMB values are given in kg m^{-2} yr^{-1}.

For further evaluation of CRYOWRF, SMB results of the regional weather model MAR have been taken into account. Simulations from MAR are taken from Agosta (2019) as described in Agosta et al. (2019). The simulations are driven by ERA-Interim (Dee et al., 2011) and cover the time period between 1979 and 2015. MAR's blowing snow module was switched off in these simulations. Details about the simulations are given in Agosta et al. (2019).

For comparison of CRYOWRF and WRF to stake measurements and MAR the model output of CRYOWRF and WRF is re-gridded to the MAR grid (35 km resolution). For each model, grid cells closest to some measurement(s) the modeled SMB is compared to the mean of all SMB measurements closest to the respective grid cell. The same averaging is performed on the WRF/CRYOWRF grid to analyze the effect of different grids. To evaluate SMB by elevation bin the averaged stake measurements as well as the modeled SMB on the respective grid cells is binned in 5 elevation bins (0–100 m (including ice shelves), 100–500 m, 500–1,000 m, 1,000–3,000 m, and >3,000 m) and averaged. To analyze the different components in CRYOWRF all land grid cells of CRYOWRF were binned and averaged for the same categories. The periods of the measurement data and the model outputs do not correspond but are based on the respective time periods of the data and simulations. This introduces some inconsistencies. However, given the 10 and 36 years of simulation for WRF/CRYOWRF and MAR, respectively, interannual variability should at least partially be removed.

3. Results and Discussion

3.1. Evaluation of Atmospheric Parameters

An evaluation of CRYOWRF against 125 (surface pressure, P), 137 (potential temperature, θ), 140 (wind speed, WSPD), and 71 (relative humidity, RH) AWS over the Antarctic continent shows reasonable correlations, mean absolute errors (MAEs) and biases for P, θ, WSPD and RH (Figure 2 and Table 1).

The statistics for CRYOWRF show comparable or better performance compared to WRF (Figure 2 and Table 1). The MAEs and the biases are lower in CRYOWRF for all tested variables. Hence, there is an improved

Table 1
Median Statistics of Correlation, Mean Absolute Error (MAE), Bias and the Difference in Standard Deviation Between the Model and the Measurements (Std. Bias) for 125, 137, 140, and 71 Stations for Surface Pressure, Potential Temperature, Wind Speed, and Relative Humidity, Respectively, Over the Antarctic Ice Sheet

Variable	Model	Correlation	MAE	Bias	Std. bias
P	WRF	0.81	5.5 hPa	1.7 hPa	0.30 hPa
	CRYOWRF	**0.82**	**5.2 hPa**	1.8 hPa	0.36 hPa
θ	WRF	0.86	6.3°C	2.0°C	1.68°C
	CRYOWRF	0.85	**4.5°C**	**−0.85°C**	−0.11°C
WSPD	WRF	0.46	3.1 m s^{-1}	−0.8 m s^{-1}	−0.94 m s^{-1}
	CRYOWRF	0.50	3.0 m s^{-1}	**−0.39 m s^{-1}**	−1.23 m s^{-1}
RH	WRF	0.20	13.0%	4.5%	0.85%
	CRYOWRF	**0.40**	**10.6%**	**0.7%**	−1.28%

Note. Statistically significant differences are marked by bold values for CRYOWRF.

representation of the absolute values (except for the bias in surface pressure). Distributions of potential temperature, θ (not shown), reveal that CRYOWRF reduces an overestimation for most stations, going along with a generally narrower distribution. For some stations CRYOWRF is not able to predict the upper end of the distribution compared to the measurements. One reason for this might be that some of these stations are located in temporally snow and ice free terrain. This underestimation of temperatures is thus likely an effect of not having snow or ice free grid cells in the model, which results in too low temperature in the model compared to measurements. However, an underestimation of the maximum temperatures is also observed for some stations on the ice shield. Overall, the standard deviation of θ is improved in CRYOWRF (−0.11°C) compared to WRF (1.68°C) with respect to the standard deviation of the measurements. For the wind speeds the standard deviation shows a slightly stronger underestimation in CRYOWRF (−1.23 m s^{-1}) compared to the measurements compared to WRF (−0.94 m s^{-1}), while the relative humidity shows significant improvement in correlation, MAE and bias with values of 0.40 (0.20), 10.6% (13.0%), and 0.7% (4.5%) for CRYOWRF (WRF). The standard deviation is strongly underestimated in CRYOWRF (−1.28%) compared to WRF (0.85%), where the standard deviation is well captured. Improvements in CRYOWRF compared to WRF can have different reasons. Some possible reasons for the improvement in CRYOWRF compared to WRF are the stability correction applied in CRYOWRF, improved representation of snow processes such as melt-freeze cycles at the surface and the representation of blowing snow.

A recent study by Mottram et al. (2021) shows correlations on the order of 0.95, 0.9 and 0.65 for surface pressure, temperature and wind speed, respectively, for simulations with the models RACMO, MAR, COSMO-CLM, HIRHAM5, and MetUM. Overall, correlations found in their study are higher compared to the correlations we present for CRYOWRF and WRF (Table 1). The reason for the differences can be manifold. The simulations analyzed in Mottram et al. (2021) cover the time period between 1979 and 2018, while our simulations are for the time period September 2010 to September 2020. Furthermore, their simulations are run with a stronger nudging approach and most of the simulations in Mottram et al. (2021) are run at a lower horizontal resolution than our simulations. Based on Mottram et al. (2021) simulations with a higher resolution are showing more divergence even if nudging is applied, because there are more grid cells in the domain which can develop the models' own dynamics, which may result in lower agreement between the model results and the measurements. Maybe most importantly, our comparison is based on hourly (3-hourly) data, while Mottram et al. (2021) rely on daily mean values. When comparing daily correlations (not shown) WRF and CRYOWRF show a performance between two model resolutions of HIRHAM5 in Mottram et al. (2021), with CRYOWRF slightly outperforming WRF irrespective of the temporal resolution (hourly, daily, monthly).

3.2. Blowing Snow in CRYOWRF

3.2.1. Drifting Snow Temporal Occurrence

Comparing the distribution of drifting snow flux in CRYOWRF to drifting snow flux measured by two 2G-FlowCapt™ sensors at the two stations D-17 and D-47 (Section 2.3) shows that drifting snow at these two

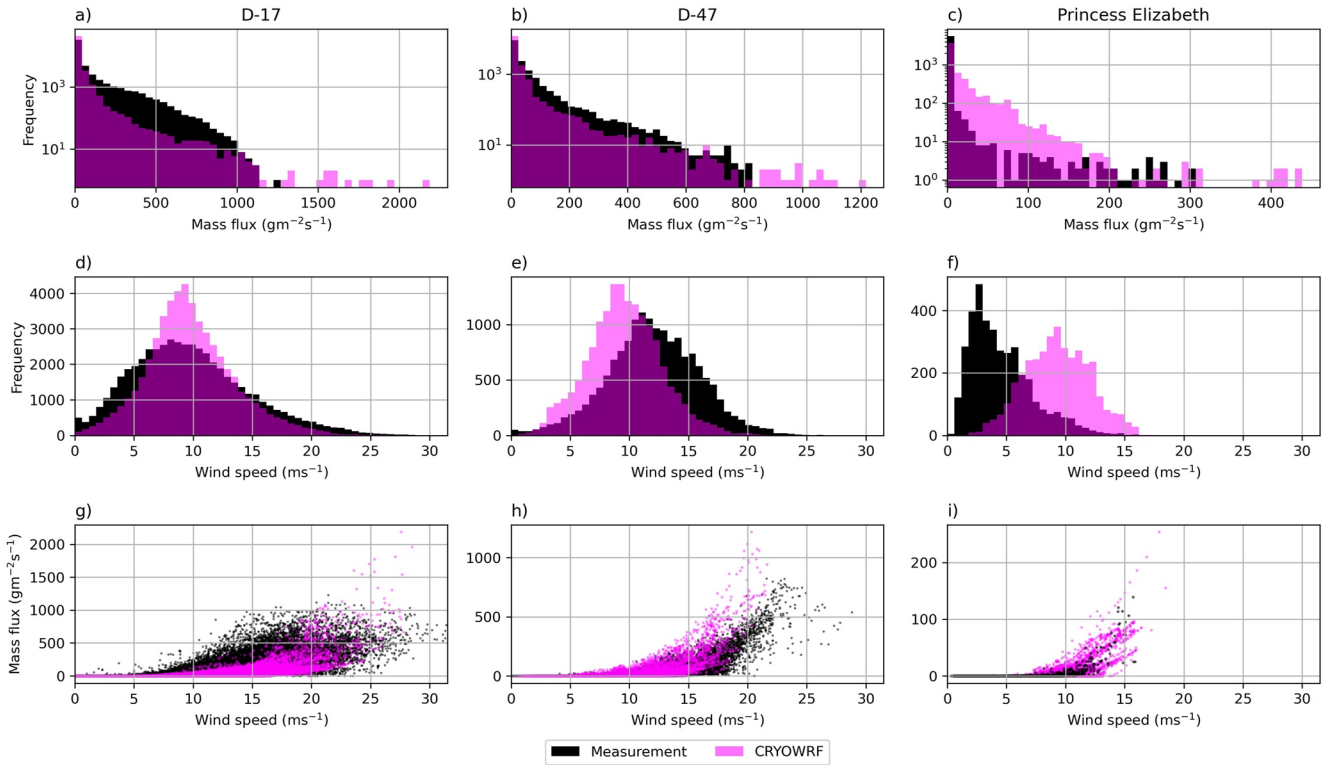

Figure 3. (a–c) Drifting snow flux distributions, (d–f) wind speed distributions and (g–i) drifting snow flux versus wind speed for the stations D-17 (left), D-47 (middle), and Princess Elizabeth (PE, right). Measurements are shown in black, CRYOWRF model output in magenta. Drifting snow flux measurements at D-17 and D-47 are performed with FlowCapt instruments, drifting snow flux measurements at PE are from a snow particle counter (SPC). Note the logarithmic *y*-axis in (a–c). Panels (g–i) are split into two panels in Figure S1 in Supporting Information S1 to display the points hidden by the data set in front.

locations is reasonably represented in CRYOWRF (Figures 3a and 3b) with a tendency to underestimate low to moderate drifting snow fluxes. However, for both locations the model shows a few high drifting snow fluxes (>1,000, >800 kg m^{-2} s^{-1} for D-17 and D-47, respectively), which are not represented in the measurements. At D-47 the shape of snow drift flux values with respect to wind speed is well represented, however, with higher drifting snow fluxes in the model compared to the measurements (Figure 3h). At D-17 the shape of the drifting snow flux versus wind speed is different between the measurement and the model and drifting snow fluxes tend to be lower in the model compared to the measurement. The yearly snow drift mass flux at D-17 is lower in the model compared to the measurements (factor 3.7). The same tendency is present at station D-47 but with a lower factor of 1.9.

In total the measurements show drifting snow for 69% (81%) of the half hourly measurements at the station D-17 (D-47). With 61% and 64% the model gives 8% (17%) less half hourly timesteps with drifting snow occurrence at the two stations D-17 and D-47, respectively. The timing of drifting snow occurrence in the model compared to the measurements is approximately 69% (66%) of the time in agreement for the station D-17 (D-47).

A further comparison has been performed with drifting snow measurements at PE station with a SPC95 in 2017 (Section 2.3). Compared to the SPC measurements CRYOWRF clearly overestimates low drifting snow fluxes (Figure 3c). However, this goes along with an overestimation of high wind speeds in the model compared to the measurements (Figure 3f) at this site. The dependency of drifting snow fluxes on wind speed is reasonably represented but the sample size for high wind speeds is low (Figure 3i).

The reasons for differences in drifting snow mass flux in the model compared to the 2G-FlowCapt™ measurements can be manifold. The blowing snow module in CRYOWRF is based on wind speed and snow properties (Section 2.1; Sharma et al., 2023; Vionnet et al., 2014). Hence, differences in wind speed and snow properties but also potential limitations in the sensor performance are likely causes for differences between the model and the measurements.

The two measurement timeseries at D-17 and D-47 show that the spread of snow drift fluxes at a given wind speed is higher at D-17 compared to D-47. This may be explained by the fact that there is more erodible snow at D-17 in winter time (Amory, 2020). Given these differences at two stations that are located apart from each other by about 100 km, it is likely that the rather coarse model resolution of 27 km cannot represent the spatial variability of snow properties between the two stations D-17 and D-47, which are an important factor for drifting and blowing snow occurrence.

Another reason for the differences is that in CRYOWRF blowing precipitation is not taken into account and blowing snow during precipitation is not well represented. While horizontally falling precipitation is measured by the sensors, it is not taken into account in the model, as precipitation is not treated on the additional blowing snow model levels below the first WRF model level. Furthermore, in reality precipitating particles hitting the ground can rebounce and eject snow particles that were deposited already and facilitate the saltation process. In CRYOWRF on the other hand all precipitating snow first deposits and looses all its kinetic energy. However, we expect the second effect to be small, as the fresh snow will be easily lifted from the ground. As D-17 is closer to the coast it may experience more precipitation and hence more events, where these mechanisms are relevant. This could explain the strong under-representation of drifting snow fluxes compared to wind speed in D-17 versus D-47.

At PE higher wind speeds in the model compared to the measurements are going along with higher drifting snow fluxes in the model compared to SPC measurements. This comparison is further limited by the fact that the SPC is mounted closer to the surface compared to the first model level in CRYOWRF.

Finally, the accuracy of the acoustic (2G-)FlowCapt^{TM} sensors is difficult to quantify (e.g., Jaedicke, 2001; Lehning et al., 2002) and the drifting or blowing snow fluxes by the second generation instruments are expected to be underestimated (Trouvilliez et al., 2015). On the other hand, no long timeseries are available from the SPC sensor. Still, lower drifting snow fluxes at D-17 in the model compared to the measurements may be caused by the missed effect of precipitation, while at D-47 lower drifting snow fluxes are rather a result of the under-representation of high wind speeds in CRYOWRF. Overall, given that drifting or blowing snow fluxes from the 2G-FlowCapt^{TM} sensors are likely underestimated and blowing snow fluxes in CRYOWRF can even be lower depending on the location, an underestimation of blowing snow fluxes may be present in the model. However, more case studies are required to confirm.

3.2.2. Continental Blowing Snow Frequency

The continental blowing snow frequency indicates a clear seasonal trend with higher blowing snow frequencies during the winter months and lower blowing snow frequencies in the summer season (Figure 4). The seasonal cycle is known and corresponds to the seasonal cycle of strong katabatic winds, which occur especially over the coastal margins of Antarctica and are driven by radiative cooling (e.g., Ball, 1956; Parish & Bromwich, 1987). Zones of a high blowing snow frequency in CRYOWRF further match zones, where wind glaze ice is present (Figure 9 in Scambos et al., 2012), for example, the Byrd–Beardmore region, the Recovery–Slessor region and the Lambert region (marked in Figure 1b). Wind glazed areas develop in regions where almost all the precipitation is removed by blowing snow and sublimation and radiative processes favor the growth of large grains (Scambos et al., 2012).

For a qualitative comparison of the blowing snow frequency in CRYOWRF to satellite measurements in Palm et al. (2018) a filtering has been applied (Section 2.1.2). The seasonal but also regional patterns of filtered blowing snow frequency in CRYOWRF (Figure 5) agree well with blowing snow frequency patterns based on satellite data (Figure 3 in Palm et al., 2018).

Both data sets show a zone of strongest blowing snow along the coast of East Antarctica with highest values of blowing snow frequency slightly inland. Zones with reduced blowing snow are found over the Amery ice shelf, toward the western Queen Maud land. Furthermore a band between Wilkes Coast and Adélie Land shows lower blowing snow frequencies in the satellite data by Palm et al. (2018). A similar structure is visible from CRYOWRF, however, slightly further to the east between Adélie Land and Victoria Land.

However, blowing snow frequencies tend to be higher in the model compared to the satellite product, especially during the summer months. This is likely due to the fact that SNOWPACK is not yet able to accurately simulate the strong sintering that happens at the surface of polar snow. This makes the snow no longer available for transport.

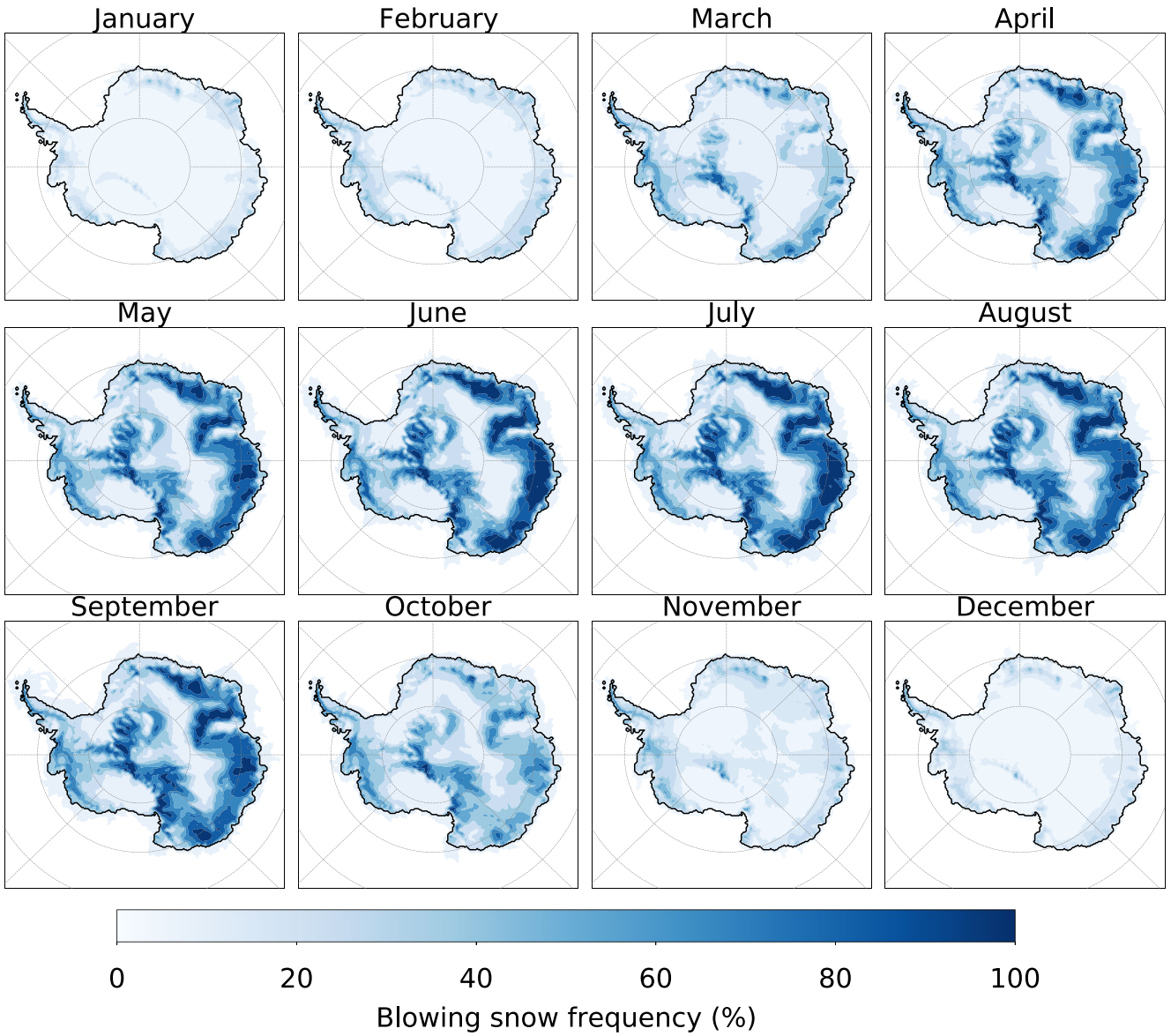

Figure 4. CRYOWRF monthly blowing snow frequency over the Antarctic continent over 10 years between 1 September 2010 and 1 September 2020.

Although CRYOWRF data is filtered, the discrepancies may further result from an under-representation of blowing snow in the satellite product, which is restricted to days with no or optically thin clouds (Section 2.1.2).

Differences between filtered and unfiltered blowing snow frequency in CRYOWRF are in the range of 0% to locally 83%. The effect of filtering is strongest in the coastal regions but generally over the regions that also show high blowing snow frequencies. Furthermore, based on our criteria filtering is much stronger in winter compared to summer. On the average over the whole continent the filtering in CRYOWRF makes up for 14% of blowing snow frequency. In coastal regions average values are 30%–50% which is slightly higher than the estimate by Palm et al. (2018) who state that their product misses about 25%–30% of East Antarctic coastal region blowing snow events. Overall, given the very different approaches, both of which have significant uncertainties, the comparison is mainly qualitative. With blowing snow frequencies in CRYOWRF comparable to blowing snow frequencies in Palm et al. (2017) and rather an underestimation of drifting snow flux at certain stations (D-17 and D-47, Section 3.2.1), drifting and blowing snow might be even higher than estimated by the model, which might go along with a higher drifting and blowing snow sublimation as discussed in Palm et al. (2017). However, further investigation is needed to confirm this hypothesis.

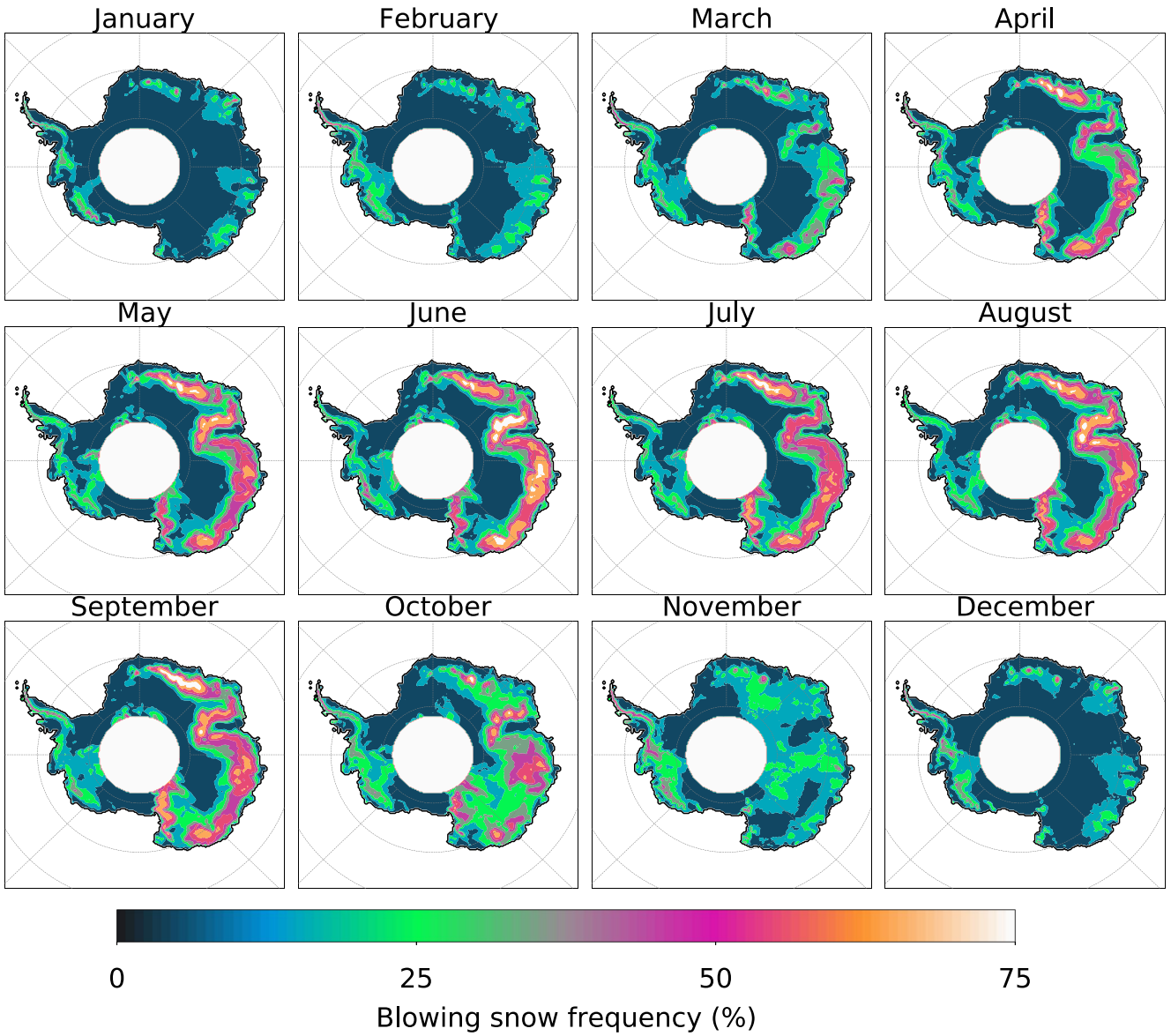

Figure 5. CRYOWRF monthly blowing snow frequency over the Antarctic continent over 10 years between 1 September 2010 and 1 September 2020, where data from the cloudiest days is removed and blowing snow has to reach at least 30 m above ground in accordance with Palm et al. (2018) (see Section 2.1.2).

3.3. SMB

3.3.1. Model Versus Stake Measurements

The simulated SMB is evaluated against stake SMB measurements over the whole continent (Section 2.4). The evaluation shows that the SMB is generally captured well by CRYOWRF (Figures 6a and 6b). The correlation of SMB between CRYOWRF and stake measurements is 0.87. This is comparable to the correlation of 0.88 between MAR and stake measurements. On the other hand, the correlation between WRF and stake measurements is with 0.58 much lower. The root mean squared error (RMSE) is similar for CRYOWRF (86.0 kg m^{-2} yr^{-1}) and MAR (77.4 kg m^{-2} yr^{-1}) compared to WRF (218.0 kg m^{-2} yr^{-1}). Especially the low SMB values (mainly from high altitude areas) are well represented in all three models. The spread of SMB values is larger in the measurements for lower altitudes between 750 and 2,500 m asl as well as below ∼100 m asl, which is also captured by CRYOWRF and MAR going along with a higher uncertainty. WRF shows strongly negative SMB below 500 m asl, which is not in agreement with the measurements. Surface mass balances at lower altitudes are overall better captured in CRYOWRF and MAR compared to WRF.

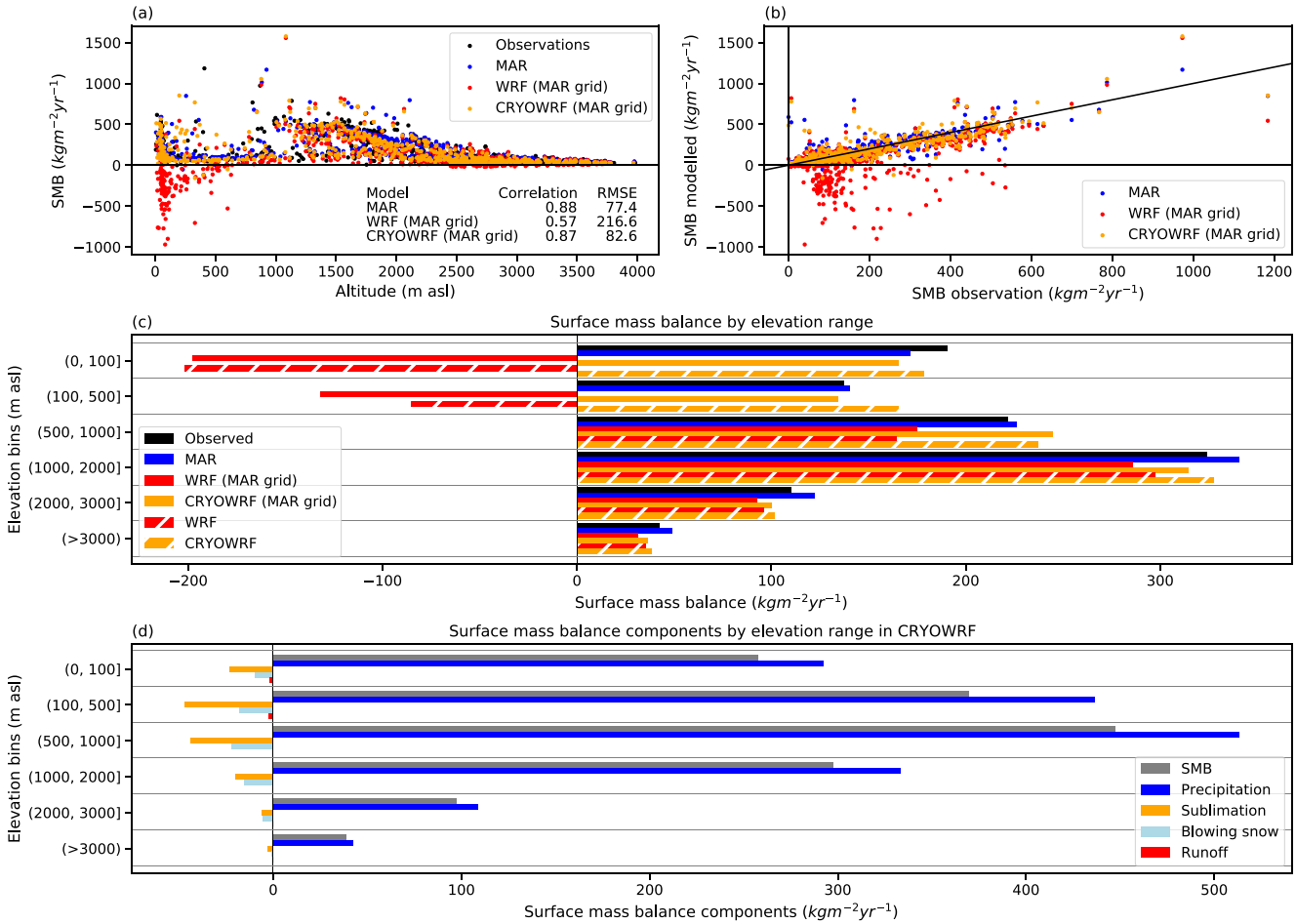

Figure 6. Evaluation of surface mass balance (SMB). (a) SMB from stake measurements (black), Modèle Atmosphéric Régional (MAR) (blue), Weather Research and Forecasting (WRF) (on MAR grid, red) and CRYOWRF (on MAR grid, orange). (b) Correlation of modeled versus measured SMB in MAR (blue), WRF (on MAR grid, red) and CRYOWRF (on MAR grid, orange). (c) Mean SMB by elevation from stake measurements (black), MAR (blue), WRF on MAR grid (red) and CRYOWRF on MAR grid (orange), WRF on WRF grid (hashed red) and CRYOWRF on WRF grid (hashed orange). (d) SMB components in CRYOWRF (on WRF grid) based on all land grid cells by elevation bin (SMB: gray, precipitation: blue, sublimation: orange, erosion: light blue, runoff: red).

When comparing SMB values by elevation bin, CRYOWRF and MAR (both on the MAR grid) show similar average SMB values compared to measurements for almost all elevation bins (Figure 6c). Correlations per elevation bin are on the same order of 0.8–0.9 for both MAR and CRYOWRF throughout all elevation bins (Table S3 in Supporting Information S1). Correlations for WRF are lower (between 0.4 and 0.7) for all elevation bins except 500–1,000 and 2,000–3,000 m asl. Root mean squared errors (RMSEs) per elevation bin are on the same order of magnitude for all elevation bins between MAR and CRYOWRF, except the elevation bin of 500–1,000 m asl, where CRYOWRF has a slightly higher RMSE (140.7 kg m^{-2} yr^{-1}) than MAR (113.4 kg m^{-2} yr^{-1}, Table S4 in Supporting Information S1). RMSEs are generally highest between 100 and 1,000 m asl $\mathcal{O}\left(110\,kgm^{-2}yr^{-1}\right)$ and lowest for the elevation bin >3,000 m asl $\mathcal{O}\left(14\,kgm^{-2}yr^{-1}\right)$. RMSEs of WRF compared to MAR and CRYOWRF are higher throughout all elevation bins with highest values in the bin between 0–100 and 100–500 m asl. Overall, WRF suffers from too strong runoff in the low altitude coastal region (negative average SMB values), which is improved by SNOWPACK, that is, CRYOWRF. The low SMB values in the elevation bins between 0–100 and 100–500 m are also the reason for the low correlation and high RMSE in WRF. For all elevation bins (except 100–500 m) average SMB values of CRYOWRF on the CRYOWRF grid improve over average SMB values of CRYOWRF on the MAR grid. However, the differences are small $\mathcal{O}\left(10\,kgm^{-2}yr^{-1}\right)$ compared to the spread of SMB values within the altitude bins $\mathcal{O}\left(100\,kgm^{-2}yr^{-1}\right)$, see Figure S3 in Supporting Information S1). Results by WRF/CRYOWRF and MAR are not fully comparable, as there are still big differences between the model setups (boundary conditions and simulation period). The idea of the comparison is to give a qualitative idea about the representation of SMB compared to another model.

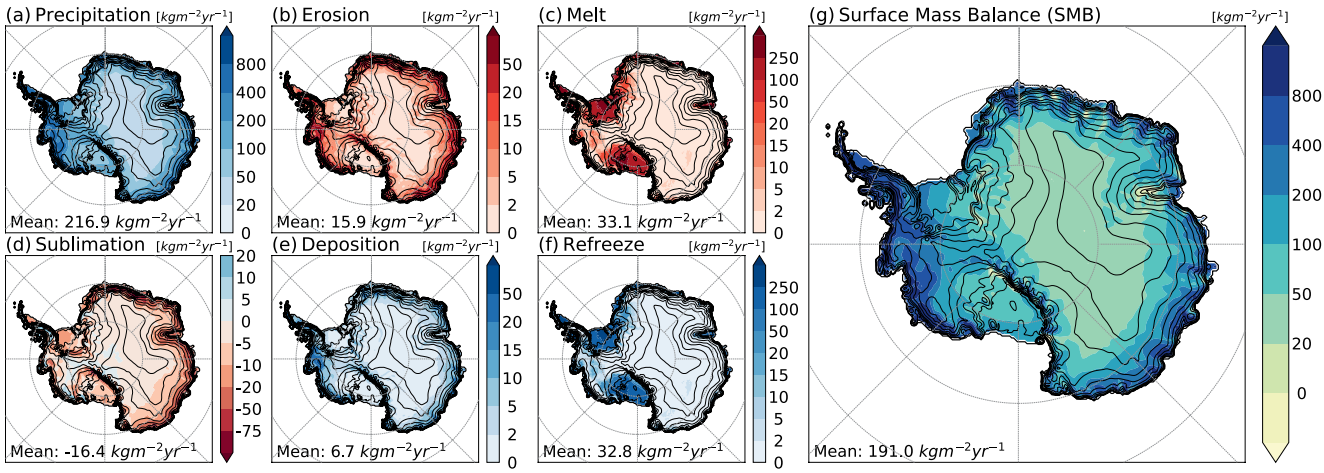

Figure 7. CRYOWRF annual mean surface mass balance (SMB) components (a–f) and SMB (g) over 10 years between 1 September 2010 and 1 September 2020.

Splitting SMB from CRYOWRF over the whole continent into its components for different altitude bins shows the contribution to SMB by the different processes (Figure 6d). The main component for mass gain is precipitation, with a peak between 500 and 1,000 m asl, correlating with the peak in SMB. The main mass loss component is surface snow sublimation. However, between 2,000 and 3,000 m asl drifting and blowing snow is about equally important. Between 1,000 and 2,000 m asl drifting and blowing snow makes up for about three quarters of surface sublimation while it still removes about half the amount of snow compared to surface snow sublimation between 500 and 1,000 m asl. The peak contribution by drifting and blowing snow is between 500 and 1,000 m asl, which is in good agreement with the regions where katabatic winds are most active as discussed in Section 3.2.2. Runoff is the smallest mass loss component and mainly important over the coastal low altitude areas, where temperatures reach the melting point most frequently.

3.3.2. SMB Annual Patterns

The annual pattern of SMB shows highest values over the peninsula, the coastal regions and the transantarctic mountains (>400 kg m^{-2} yr^{-1}, Figure 7). Lowest SMB values are present over the central ice sheet (<50 kg m^{-2} yr^{-1}). The pattern and range of values is in good agreement with the SMB distribution presented based on MAR simulations in Figure 1 in Agosta et al. (2019) with highest values over the peninsula, coastal regions and the transantarctic mountains (SMB >200–400 kg m^{-2} yr^{-1}) and lowest values over central Antarctica (SMB <50 kg m^{-2} yr^{-1}). Smaller scale SMB structures in CRYOWRF are mainly visible along the coasts, the transantarctic mountains and the Ronne embayment. In the region of the latter, there may be a contribution by drifting and blowing snow as we can see distinct patterns of drifting and blowing snow in this region (Figure 7b). Furthermore, as shown in Section 3.2.2, drifting and blowing snow is mostly active in the katabatic regions and along the transantarctic mountains (Figure 7b). Surface snow sublimation is most effective in the coastal regions (<−50 kg m^{-2} yr^{-1}, Figure 7d). In the interior of the continent, the Antarctic Peninsula and West Antarctica there are regions, where deposition dominates over sublimation in the annual mean (blue regions in Figure 7d). This most likely is an effect of the low temperatures, for which saturation is reached at very low humidity levels. Finally, melt is strongest in the coastal regions and over the big ice shelves. Most of the melt refreezes (Figure 7f) and hence the contribution by runoff (melt minus refreeze) on the total SMB is rather small (see Section 3.4). Melt and refreeze processes are stronger over West Antarctica compared to East Antarctica.

3.4. What Is the Impact of Drifting and Blowing Snow on SMB at a 27 km Resolution?

Based on CRYOWRF drifting and blowing snow removes 4.2% of the annual precipitation over the Antarctic continent on average (Table 2). This is more than half of the amount of snow removed by surface sublimation. Runoff on the other hand only removes 0.2% of the annual precipitation on a continental scale. Loss of surface mass by drifting and blowing snow can occur due to two reasons. Either snow is blown off the continent or it sublimates during redistribution. From our analysis 1.0% of the annual precipitation is blown off the continent

Table 2
Surface Mass Balance (SMB) Components and Their Relative Contribution to SMB

Component	Amount (Gt yr^{-1})	Percent. of SMB (%)	Percent. of precip. (%)
Precipitation	3,101.2	113.6	–
Surface sublimation	234.0	8.6	7.5
Runoff	5.1	0.2	0.2
Blowing snow	131.7	4.8	4.3
Off continent	30.7	1.1	1.0
Sublimation	100.9	3.7	3.3
SMB	2,730.1	–	88.0

Note. The runoff contribution is calculated from melt minus refreeze. Equivalently, the loss by drifting and blowing snow (blowing snow) is calculated as erosion minus deposition. Percent. means percentage, precip. means precipitation.

(i.e., blowing snow deposited off continent on sea grid cells), while 3.3% of the annual precipitation are lost due to drifting and blowing snow sublimation (i.e., the difference of snow eroded over land and deposited over land or sea grid cells). In total about 12% of the annual precipitation are removed by all processes. With 4.2% of the annual precipitation being removed by drifting and blowing snow (either drifting and blowing snow sublimation or snow blown off the continent), drifting and blowing snow makes up for about one third of the total loss of precipitation and hence significantly influences the SMB of Antarctica.

Compared to the results by Agosta et al. (2019), the percentages of mass removal by drifting and blowing snow compared to SMB are comparable between RACMO (4.8%) and CRYOWRF (4.8%), while CRYOWRF suggests higher surface sublimation rates (8.6%, RACMO: 2.6%). With 5% mass removal by surface sublimation with respect to SMB, MAR lies in between. Compared to precipitation the percentages of surface sublimation are 7.5%, 2.4% and 4.8% for CRYOWRF, RACMO, and MAR, respectively, that is, on a similar order of magnitude as compared to SMB, which means the differences are not compensated by precipitation. However, the estimates by Agosta et al. (2019) for drifting and blowing snow only apply for the AIS without the peninsula, while the estimates for CRYOWRF are representative for the whole continent including the peninsula. Furthermore, the simulations are driven by different boundary conditions (ERA-5 for CRYOWRF and ERA-interim for RACMO and MAR) and do not cover the same period of time. Therefore, the comparisons are not fully valid and parts of the higher percentage might be due to including the peninsula in CRYOWRF as well as different boundary conditions. Given that precipitation is high in the peninsula compared to the majority of the continent and sublimation over the mountains of the peninsula is even positive (i.e., net deposition, Figure 7d), the effect might not compensate for the differences between the models. However, for a quantitative comparison simulations of the same period, on the same grid with the same boundary conditions would be needed. Given that the annual drifting snow fluxes in CRYOWRF compared to the FlowCapt measurements at D-17 and D-47 are rather underestimated (Section 2.1.1) the estimation of the snow flux in CRYOWRF may be conservative. To get a more complete picture of the performance of CRYOWRF in representing drifting and blowing snow flux additional measurements need to be compared in the future. Furthermore, the uncertainty of the measurements is an additional caveat. Based on the comparison of blowing snow frequency patterns compared to satellite measurements (Section 3.2.2) it is expected, that CRYOWRF seems to reasonably represent blowing snow frequency patterns. However, it is strongly dependent on the location and season, whether the simulation rather over- or underestimates the blowing snow frequency compared to the satellite measurements in Palm et al. (2018). Additionally, the comparison of blowing snow frequency to Palm et al. (2018) in this study is only qualitative given that the estimates are based on a blowing snow mixing ratio threshold of 10^{-7} kg kg^{-1} and a reduction of blowing snow due to overcast conditions based on the terrain altitude. Furthermore, the satellite measurements are also affected by uncertainties.

4. Conclusion and Outlook

CRYOWRF, a recently developed version of WRF with a blowing snow module that is coupled to the snow model SNOWPACK (Sharma et al., 2023) is assessed based on a 10-year simulation over the Antarctic continent. At

a point scale, CRYOWRF shows a good representation of atmospheric conditions with respect to AWS measurements. Compared to WRF using the surface model (Noah-MP, state-of-the-art) a significant reduction in the bias and MAE of the potential temperature as well as relative humidity are observed. This is likely related to the improved representation of the snow surface by the snow model SNOWPACK, which is used as surface model in CRYOWRF. Compared to Noah-MP, SNOWPACK is based on several 100 snow layers (compared to 3 layers in Noah-MP). Furthermore, it is a state-of-the-art snow model taking into account grain properties of the snowpack.

In addition to a state-of-the-art snow surface model the capability to consider blowing snow is an important feature of CRYOWRF. Hence, an evaluation of drifting and blowing snow is performed for snow drift measurements at point scale as well as blowing snow frequency on a continental scale. The blowing snow scheme is based on (Vionnet et al., 2014) and was previously found to rather overestimate blowing snow fluxes. Our model evaluation shows that an overestimation may be present in certain regions, while in other regions, the missing influence of precipitation and its ability of initiating the saltation process and subsequently drifting and blowing snow, rather leads to an underestimation of drifting snow fluxes compared to wind speed. Moreover, blowing snow frequency is underestimated in CRYOWRF by 8%–17% compared to FlowCapt measurements in Adélie land. More data needs to be analyzed in future studies for final conclusions.

CRYOWRF is based on a sophisticated snow model (SNOWPACK) the blowing snow module is based on Vionnet et al. (2014), which—as most of the saltation parameterizations used in mesoscale models—is based on steady state saltation assuming an equilibrium between the wind field and the grains in motion (Doorschot & Lehning, 2002; Sørensen, 2004). Additionally, Melo et al. (2022) show in a recent study that a proper representation of the grain size distribution and cohesion of the snow grains are crucial to model saltation fluxes. Based on the high uncertainty of the parameters used in the saltation model the mass flux of drifting and blowing snow may not be adequate, which also affects the estimates of drifting and blowing snow sublimation and the mass of snow blown off the continent. Further inaccuracy arises from neglecting the contribution of horizontal precipitation advection, which often occurs together with drifting and blowing snow events. Additionally, the neglected effect of precipitation ejecting particles when impacting and the model resolution of 27 km is too coarse to capture the small-scale nature of the drifting and blowing snow process.

While not all aspects of drifting and blowing snow are properly represented, the current results by CRYOWRF confirm that drifting and blowing snow losses have a significant influence on the total SMB of Antarctica, as discussed previously (e.g., Agosta et al., 2019) and CRYOWRF seems to properly represent the general patterns of blowing snow frequency on a continental scale, compared to satellite measurements (Palm et al., 2018). The general pattern of drifting snow mass flux versus wind speed is fairly represented but shows different deficiencies for different locations, which may be explained by the coarse model resolution or the process representation. For an improved representation of drifting and blowing snow in CRYOWRF the implementation of a grain size distribution and cohesion-aware saltation model will be crucial. It is planned to implement a saltation model in CRYOWRF based on the results by Melo et al. (2022). As a next important step, we will also apply CRYOWRF at much higher resolution to specific target regions of the Antarctic continent. We expect scale-dependency of the highly non-linear process of drifting and blowing snow sublimation (Sigmund et al., 2022) but also of local to regional divergence of the mass flux. At higher resolution, the influence of the blowing snow cloud on precipitation processes can also be investigated and will be a focus of future research.

Data Availability Statement

CRYOWRF v1.0 is publicly available under the GPL v3 License. The code is available on the institutional repository (CRYOWRF, 2023). CRYOWRF v1.0 is based on WRF version 4.2 (WRF, 2023). Surface mass balance measurements and processing scripts were used from Agosta et al. (2019). MAR model results can be downloaded from Agosta and Fettweis (2019), while the SMB observations and python scripts are available from Agosta (2019). AWS and blowing snow data was downloaded from several databases as listed below and in the Acknowledgments section. Blowing snow data from PE station can be made available upon request. Databases from which AWS data was collected: AMRC, Lazzara et al. (2012); AAD, Barnes-Keoghan (2000); Antarctic Meteo-Climatological Observatory by the Italian National Programme of Antarctic Research, CLIMANTARTIDE (PNRA, 2020); National Oceanic and Atmospheric Administration, NOAA (NOAA, 2021); World Data Center PANGAEA, for example, König-Langlo (2012); Japan Meteorological Agency, JMA (JMA, 2020); Princess Elisabeth, PE, KU Leuven (Gorodetskaya et al., 2013; Gorodetskaya et al., 2015, the data can be made

Acknowledgments
For supporting us with computing resources by granting the projects s873, s938, and s1115 we thank the Swiss National Supercomputer Center (CSCS). Science was mainly funded by the ENAC big call grant of EPFL (project LOSUMEA) and the Swiss National Science Foundation (SNF) project "From cloud to ground: Snow deposition in extreme environments" (Grant: 179130). We thank our project partners in LOSUMEA, Prof. Alexis Berne and Dr. Etienne Vignon for many fruitful discussions. For providing us with the IMAU-FDM data, which was used to initialize CRYOWRF, we thank Dr. Peter Munneke of the Institute of Marine and Atmosphere research (IMAU), Utrecht University. Furthermore, we are grateful to the Free and Open-source software community. The python packages wrf-python, xarray, pandas, matplotlib have greatly supported our data analysis. AWS data were obtained from different data platforms. Hence, we would like to thank the Antarctic Meteo-Climatological Observatory at MZS and Victoria Land of PNRA, http://www.climantartide.it. Data for the AWS station D-17 and D-47 was kindly provided by Dr. Charles Amory. For the station South Pole we use measurement data provided by the National Oceanic and Atmospheric Administration (NOAA) Global Monitoring Laboratory. Furthermore, the authors appreciate the support of the Automatic Weather Station Program AMRC (Prof. Matthew Lazzara, NSF grants number ANT-0944018 and ANT-1924730). We kindly thank the IMAU and in particular Dr. C. J. P. P. Smeets for preparing and providing the data of several weather stations of their network. The station data of the Syowa station was retrieved from the online database by the Japanese Antarctic Research expedition (JARE) at the Japanese Antarctic stations from 1957 to 2018, whom we thank for keeping the data open access at https://www.data.jma.go.jp/antarctic/datareport/index-e.html. For AWS data of multiple stations we thank the Australian Antarctic Data Centre, the AAD and the Bureau of Meteorology, Australia. We kindly thank the AWI for providing AWS data of the Neumayer station on the PANGAEA data publisher for Earth & Environmental Science platform. Furthermore, we would like to acknowledge KU Leuven, and Prof. Nicole van Lipzig and Dr. Alexandra Gossart in particular, for providing us with AWS data of Princess Elisabeth station. Finally, we would like to thank the British Antarctic Survey (BAS) for collecting AWS data from different sources and making it openly available and all the individual data providers contributing to the database. Furthermore, we would like to thank C. Agosta for making the SMB data, model output and code used in Agosta et al. (2019) publicly available upon request by Prof. N. van Lipzig, KU Leuven); Stations D-17 and D-47 in a transect between Dumont d'Urville and Dome C (Amory, 2020); Institute for Marine and Atmospheric Research Utrecht, IMAU (IMAU, 2021); and the British Antarctic Survey, BAS (BAS, 2021). Python (especially packages wrf-python, xarray, pandas, matplotlib) was used extensively. The corresponding code and preprocessed simulation output as well as information about the simulation setup are publicly available from Gerber et al. (2022). Python software to preprocess AWS data is available from Gerber and Lehning (2022).

References

Agosta, C. (2019). Agosta et al. (2019), The cryosphere: Data processing, analyses and figures [Software]. Zenodo. http://doi.org/10.5281/zenodo.2548848

Agosta, C., Amory, C., Kittel, C., Orsi, A., Favier, V., Gallée, H., et al. (2019). Estimation of the Antarctic surface mass balance using the regional climate model MAR (1979–2015) and identification of dominant processes. *The Cryosphere*, *13*(1), 281–296. https://doi.org/10.5194/tc-13-281-2019

Agosta, C., & Fettweis, X. (2019). Antarctic surface mass balance with the regional climate model MAR (1979-2015) [Software and Dataset]. Zenodo. http://doi.org/10.5281/zenodo.2547638

Amory, C. (2020). Drifting-snow statistics from multiple-year autonomous measurements in Adélie Land, East Antarctica. *The Cryosphere*, *14*(5), 1713–1725. https://doi.org/10.5194/tc-14-1713-2020

Amory, C., Kittel, C., Le Toumelin, L., Agosta, C., Delhasse, A., Favier, V., & Fettweis, X. (2021). Performance of MAR (v3.11) in simulating the drifting-snow climate and surface mass balance of Adélie Land, East Antarctica. *Geoscientific Model Development*, *14*(6), 3487–3510. https://doi.org/10.5194/gmd-14-3487-2021

Ball, F. K. (1956). The theory of strong katabatic winds. *Australian Journal of Physics*, *9*(3), 373–386. https://doi.org/10.1071/PH560373

Barnes-Keoghan, I. (2000). Antarctic Climate data collected by Australian agencies, ver. 1 [Dataset]. Australian Antarctic Data Centre. Retrieved from https://data.aad.gov.au/metadata/records/Antarctic_Meteorology

BAS. (2021). AWS data Antarctica [Dataset]. British Antarctic Survey (BAS). Retrieved from https://legacy.bas.ac.uk/met/READER/ANTARCTIC_METEOROLOGICAL_DATA/SURFACE/surface_index.html;ftp://ftp.bas.ac.uk/src/ANTARCTIC_METEOROLOGICAL_DATA/AWS/

CRYOWRF. (2023). CRYOWRF repository—Latest updates [Software]. CRYOWRF. Retrieved from https://gitlabext.wsl.ch/atmospheric-models/CRYOWRF/-/tags/v1.0

Dee, D. P., Uppala, S. M., Simmons, A. J., Berrisford, P., Poli, P., Kobayashi, S., et al. (2011). The Era-Interim reanalysis: Configuration and performance of the data assimilation system. *The Quarterly Journal of the Royal Meteorological Society*, *137*(656), 553–597. https://doi.org/10.1002/qj.828

Doorschot, J. J. J., & Lehning, M. (2002). Equilibrium saltation: Mass fluxes, aerodynamic entrainment, and dependence on grain properties. *Boundary-Layer Meteorology*, *104*(1), 111–130. https://doi.org/10.1023/A:1015516420286

Favier, V., Agosta, C., Parouty, S., Durand, G., Delaygue, G., Gallée, H., et al. (2013). An updated and quality controlled surface mass balance dataset for Antarctica. *The Cryosphere*, *7*(2), 583–597. https://doi.org/10.5194/tc-7-583-2013

Fretwell, P., Pritchard, H. D., Vaughan, D. G., Bamber, J. L., Barrand, N. E., Bell, R., et al. (2013). Bedmap2: Improved ice bed, surface and thickness datasets for Antarctica. *The Cryosphere*, *7*(1), 375–393. https://doi.org/10.5194/tc-7-375-2013

Frezzotti, M. P., Flora, O., Gandolfi, S., Gay, M., Urbini, S., & Fily, M. (2004). New estimations of precipitation and surface sublimation in East Antarctica from snow accumulation measurements. *Climate Dynamics*, *23*(7–8), 803–813. https://doi.org/10.1007/s00382-004-0462-5

Gallée, H., Trouvilliez, A., Agosta, C., Genthon, C., Favier, V., & Naaim-Bouvet, F. (2013). Transport of snow by the wind: A comparison between observations in Adélie Land, Antarctica, and simulations made with the regional climate model MAR. *Boundary-Layer Meteorology*, *146*(1), 133–147. https://doi.org/10.1007/s10546-012-9764-z

Gerber, F., & Lehning, M. (2020). REMA topography and AntarcticaLC2000 for WRF [documentation. *EnviDat*. https://doi.org/10.16904/envidat.190

Gerber, F., & Lehning, M. (2022). Preprocessing Antarctic Weather Station (AWS) data in python [Computational Notebooks]. *EnviDat*. https://doi.org/10.16904/envidat.340

Gerber, F., Sharma, V., & Lehning, M. (2022). Reproducibility dataset for CRYOWRF validation [Dataset and Computational Notebooks]. *EnviDat*. https://doi.org/10.16904/envidat.347

Gorodetskaya, I., Kneifel, S., Maahn, M., Van Tricht, K., Thiery, W., Schween, J., et al. (2015). Cloud and precipitation properties from ground-based remote-sensing instruments in East Antarctica. *The Cryosphere*, *9*(1), 285–304. https://doi.org/10.5194/tc-9-285-2015

Gorodetskaya, I., Van Lipzig, N., Broeke, V. D., Manold, A., Boot, W., & Reijmer, C. (2013). Meteorological regimes and accumulation patterns at Utsteinen, Dronning Maud Land, East Antarctica: Analysis of two contrasting years. *Journal of Geophysical Research*, *118*(4), 1700–1715. https://doi.org/10.1002/jgrd.50177

Gossart, A., Palm, S. P., Souverijns, N., Lenaerts, J. T. M., Gorodetskaya, I. V., Lhermitte, S., & van Lipzig, N. P. M. (2020). Importance of blowing snow during cloudy conditions in East Antarctica: Comparison of ground-based and space-borne retrievals over ice-shelf and mountain regions. *Frontiers in Earth Science*, *8*, 240. https://doi.org/10.3389/feart.2020.00240

Gossart, A., Souverijns, N., Gorodetskays, I. V., Lhermitte, S., Lenaerts, J. T. M., Schween, J. H., et al. (2017). Blowing snow detection from ground-based ceilometers: Application to East Antarctica. *The Cryosphere*, *11*(6), 2755–2772. https://doi.org/10.5194/tc-11-2755-2017

Hersbach, H., Bell, B., Berrisford, P., Biavati, G., Horányi, A., Muñoz Sabater, J., et al. (2018a). *ERA5 hourly data on pressure levels from 1979 to present*. Copernicus Climate Change Service (C3S) Climate Data Store (CDS). https://doi.org/10.24381/cds.bd0915c6

Hersbach, H., Bell, B., Berrisford, P., Biavati, G., Horányi, A., Muñoz Sabater, J., et al. (2018b). *ERA5 hourly data on single levels from 1979 to present*. Copernicus Climate Change Service (C3S) Climate Data Store (CDS). https://doi.org/10.24381/cds.adbb2d47

Hofer, S., Amory, C., Kittel, C., Carlsen, T., Le Toumelin, L., & Storelvmo, T. (2021). The contribution of drifting snow to cloud properties and the atmospheric radiative budget over Antarctica. *Geophysical Research Letters*, *48*(22), e2021GL094967. https://doi.org/10.1029/2021GL094967

Holtslag, A. A. M., & De Bruin, H. A. R. (1988). Applied modeling of the nighttime surface energy balance over land. *Journal of Applied Meteorology*, *27*(6), 689–704. https://doi.org/10.1175/1520-0450(1988)027⟨0689:AMOTNS⟩2.0.CO;2

Howat, I. M., Porter, C., Smith, B. E., Noh, M.-J., & Morin, P. (2019). The reference elevation model of Antarctica. *The Cryosphere*, *13*(2), 665–674. https://doi.org/10.5194/tc-13-665-2019

Hui, F., Kang, J., Liu, Y., Cheng, X., Gong, P., Wang, F., et al. (2017). AntarcticaLC2000: The new Antarctic land cover database for the year 2000. *Science China Earth Sciences*, *60*(4), 686–696. https://doi.org/10.1007/s11430-016-0029-2

available. Finally, we thank Aaron Kennedy and two anonymous reviewers for their constructive comments which helped us to improve the paper. Open access funding provided by ETH-Bereich Forschungsanstalten.

IMAU. (2021). Ice and climate: Polar in-situ observations [Dataset]. Institute for Marine and Atmospheric Research Utrecht. Retrieved from https://www.projects.science.uu.nl/iceclimate/aws/antarctica.php;https://www.projects.science.uu.nl/iceclimate/aws/index.php

Jaedicke, C. (2001). Acoustic snowdrift measurements: Experiences from the FlowCapt instrument. *Cold Regions Science and Technology*, *32*(1), 71–81. https://doi.org/10.1016/S0165-232X(01)00017-9

Jensen, A. A., Harrington, J. Y., Morrison, H., & Milbrandt, J. A. (2017). Predicting ice shape evolution in a bulk microphysics model. *Journal of the Atmospheric Sciences*, *74*(6), 2081–2104. https://doi.org/10.1175/JAS-D-16-0350.1

JMA. (2020). Antarctic Meteorological Data [Dataset]. JMA. Retrieved from https://www.data.jma.go.jp/antarctic/datareport/index-e.htm

König-Langlo, G. (2012). Continuous meteorological observations at Neumayer station (2011-01) [Dataset]. Alfred Wegener Institute, Helmholtz Centre for Polar and Marine Research, Bremerhaven, PANGAEA. https://doi.org/10.1594/PANGAEA.775173

Lazzara, M., Weidner, G., Keller, L., Thom, J., & Cassano, J. (2012). Antarctic automatic weather station program: 30 years of polar observations [Dataset]. Bulletin of the American Meteorological Society, *93*(10), 1519–1537. https://doi.org/10.1175/BAMS-D-11-00015.1

Lehning, M., Bartelt, P., Brown, B., Russi, T., Stöckli, U., & Zimmerli, M. (1999). SNOWPACK model calculations for avalanche warning based upon a new network of weather and snow stations. *Cold Regions Science and Technology*, *30*(1–3), 145–157. https://doi.org/10.1016/S0165-232x(99)00022-1

Lehning, M., Doorschot, J., & Bartelt, P. (2000). A snowdrift index based on SNOWPACK model calculations. *Annals of Glaciology*, *31*, 382–386. https://doi.org/10.3189/172756400781819770

Lehning, M., Naaim, F., Naaim, M., Brabec, B., Doorschot, J., Durand, Y., et al. (2002). Snow drift: Acoustic sensors for avalanche warning and research. *Natural Hazards and Earth System Sciences*, *2*(3/4), 121–128. https://doi.org/10.5194/nhess-2-121-2002

Lenaerts, J. T. M., van den Broeke, M. R., Déry, S. J., van Meijgaard, E., van de Berg, W. J., Palm, S. P., & Sanz Rodrigo, J. (2012). Modeling drifting snow in Antarctica with a regional climate model: 1. Methods and model evaluation. *Journal of Geophysical Research*, *117*, D05108. https://doi.org/10.1029/2011JD016145

Letcher, T. W., LeGrand, S. L., & Polashenski, C. (2021). Applying a physically based blowing snow diagnostic parameterization to improve wintertime visibility forecasts in the WRF model. *Weather and Forecasting*, *36*(2), 615–626. https://doi.org/10.1175/WAF-D-20-0106.1

Ligtenberg, S. R. M., Helsen, M. M., & van den Broeke, M. R. (2011). An improved semi-empirical model for the densification of Antarctic firn. *The Cryosphere*, *5*(4), 809–819. https://doi.org/10.5194/tc-5-809-2011

Loeb, N. A., & Kennedy, A. (2021). Blowing snow at McMurdo station, Antarctica during the AWARE field campaign: Surface and ceilometer observations. *Journal of Geophysical Research: Atmospheres*, *126*(7), e2020JD033935. https://doi.org/10.1029/2020JD033935

Medley, B., Joughin, I., Smith, B. E., Das, S. B., Steig, E. J., Conway, H., et al. (2014). Constraining the recent mass balance of Pine Island and Thwaites glaciers, West Antarctica, with airborne observations of snow accumulation. *The Cryosphere*, *8*(4), 1375–1392. https://doi.org/10.5194/tc-8-1375-2014

Melo, D. B., Sharma, V., Comola, F., Sigmund, A., & Lehning, M. (2022). Modeling snow saltation: The effect of grain size and interparticle cohesion. *Journal of Geophysical ResearchAtmospheres*, *172*(1), e2021JD035260. https://doi.org/10.1029/2021JD035260

Morrison, H., Curry, J. A., & Khvorostyanov, V. I. (2005). A new double-moment microphysics parameterization for application in cloud and climate models. Part I: Description. *Journal of the Atmospheric Sciences*, *62*(6), 1665–1677. https://doi.org/10.1175/JAS3446.1

Morrison, H., Thompson, G., & Tatarskii, V. (2009). Impact of cloud microphysics on the development of trailing stratiform precipitation in a simulated squall line: Comparison of one- and two-moment schemes. *Monthly Weather Review*, *137*(3), 991–1007. https://doi.org/10.1175/2008MWR2556.1

Mottram, R., Hansen, N., Kittel, C., van Wessem, J. M., Agosta, C., Amory, C., et al. (2021). What is the surface mass balance of Antarctica? An intercomparison of regional climate model estimates. *The Cryosphere*, *15*(8), 3751–3784. https://doi.org/10.5194/tc-15-3751-2021

Munneke, P. K., van den Broeke, M. R., Lenaerts, J. T. M., Flanner, M. G., Gardner, A. S., & van de Berg, W. J. (2011). A new albedo parameterization for use in climate models over the Antarctic ice sheet. *Journal of Geophysical Research*, *116*(D5), D05114. https://doi.org/10.1029/2010JD015113

Nakanishi, M., & Niino, H. (2006). An improved Mellor–Yamada level 3 model: Its numerical stability and application to a regional prediction of advecting fog. *Boundary-Layer Meteorology*, *119*(2), 397–407. https://doi.org/10.1007/s10546-005-9030-8

Nakanishi, M., & Niino, H. (2009). Development of an improved turbulence closure model for the atmospheric boundary layer. *Journal of the Meteorological Society of Japan*, *87*(5), 895–912. https://doi.org/10.2151/jmsj.87.895

Niu, G.-Y., Yang, Z.-L., Mitchell, K. E., Chen, F., Ek, M. B., Barlage, M., et al. (2011). The community Noah land surface model with multiparameterization options (Noah-MP): 1. Model description and evaluation with local-scale measurements. *Journal of Geophysical Research*, *116*(D12), D12109. https://doi.org/10.1029/2010JD015139

NOAA. (2021). Meteorology measurements from the National Oceanic and Atmospheric Administration [Dataset]. (NOAA)/Earth System Research Laboratory (ESRL)/Global Monitoring Division (GMD) Baseline Observatories. Retrieved from https://gml.noaa.gov/aftp/data/meteorology/in-situ/spo/

Palm, S. P., Kayetha, V., & Yang, Y. (2018). Toward a satellite-derived climatology of blowing snow over Antarctica. *Journal of Geophysical Research Atmospheres*, *123*(18), 10301–10313. https://doi.org/10.1029/2018JD028632

Palm, S. P., Kayetha, V., Yang, Y., & Pauly, R. (2017). Blowing snow sublimation and transport over Antarctica from 11 years of CALIPSO observations. *The Cryosphere*, *11*(6), 2555–2569. https://doi.org/10.5194/tc-11-2555-2017

Parish, T. R., & Bromwich, D. H. (1987). The surface windfield over the Antarctic ice sheets. *Nature*, *328*(6125), 51–54. https://doi.org/10.1038/328051a0

PNRA. (2020). Observatory hourly AWS data by the Antarctic meteo-climatological observatory at MZS and Victoria land (PNRA) [Dataset]. Data and information were obtained from 'MeteoClimatological Observatory at MZS and Victoria Land' of PNRA. Retrieved from http://www.climantartide.it

Scambos, T. A., Frezzotti, M., Haran, T., Bohlander, J., Lenaerts, J. T. M., Van Den Broeke, M. R., et al. (2012). Extent of low-accumulation 'wind glaze' areas on the East Antarctic plateau: Implications for continental ice mass balance. *Journal of Glaciology*, *58*(210), 633–647. https://doi.org/10.3189/2012JoG11J232

Schmidt, R. A. (1980). Threshold wind-speeds and elastic impact in snow transport. *Journal of Glaciology*, *26*(94), 453–467. https://doi.org/10.3189/S0022143000010972

Sharma, V., Gerber, F., & Lehning, M. (2023). Introducing CRYOWRF v1.0: Multiscale atmospheric flow simulations with advanced snow cover modelling. *Geoscientific Model Development*, *16*(2), 719–749. https://doi.org/10.5194/gmd-16-719-2023

Sigmund, A., Dujardin, J., Comola, F., Sharma, V., Huwald, H., Melo, D. B., et al. (2022). Evidence of strong flux underestimation by bulk parametrizations during drifting and blowing snow. *Boundary-Layer Meteorology*, *128*(1), 119–146. https://doi.org/10.1007/s10546-021-00653-x

Skamarock, Klemp, J. B., Dudhia, J., Gill, D. O., Liu, Z., Berner, J., et al. (2019). *A description of the advanced research WRF version 4.1 (no. ncar/tn-556+str) (Tech. Rep.)*. Mesoscale and Microscale Meteorological Division, National Center for Atmospheric Research. https://doi.org/10.5065/1dfh-6p97

Smith, B., Fricker, H. A., Gardner, A. S., Medley, B., Nilsson, J., Paolo, F. S., et al. (2020). Pervasive ice sheet mass loss reflects competing ocean and atmosphere processes. *Science*, *368*(6496), 1239–1242. https://doi.org/10.1126/science.aaz5845

Sørensen, M. (2004). On the rate of aeolian sand transport. *Geomorphology*, *59*(1–4), 59–62. https://doi.org/10.1016/j.geomorph.2003.09.005

Steger, C. R., Reijmer, C. H., van den Broeke, M. R., Wever, N., Forster, R. R., Koenig, L. S., et al. (2017). Firn meltwater retention on the Greenland ice sheet: A model comparison. *Frontiers in Earth Science*, *5*, 3. https://doi.org/10.3389/feart.2017.00003

Trouvilliez, A., Naaim-Bouvet, F., Bellot, H., Genthon, C., & Gallée, H. (2015). Evaluation of the FlowCapt acoustic sensor for the aeolian transport of snow. *Journal of Atmospheric and Oceanic Technology*, *32*(9), 1641. https://doi.org/10.1175/JTECH-D-14-00104.1

van den Broeke, M. R., van Lipzip, N. P. M., & van Meijgaard, E. (2002). Momentum budget of the East Antarctic atmospheric boundary layer: Results of a regional climate model. *Journal of the Atmospheric Sciences*, *59*(21), 3117–3129. https://doi.org/10.1175/1520-0469(2002)059⟨3117:MBOTEA⟩2.0.CO;2

van Wessem, J. M., van de Berg, W. J., Noël, B. P. Y., van Meijgaard, E., Amory, C., Birnbaum, G., et al. (2018). Modelling the climate and surface mass balance of polar ice sheets using RACMO2—Part 2: Antarctica (1979–2016). *The Cryosphere*, *12*(4), 1479–1498. https://doi.org/10.5194/tc-12-1479-2018

Vaughan, D. G., Bamber, J. L., Giovinetto, M., Russell, J., & Cooper, A. P. R. (1999). Reassessment of net surface mass balance in Antarctica. *Journal of Climate*, *12*(4), 933–946. https://doi.org/10.1175/1520-0442(1999)012⟨0933:RONSMB⟩2.0.CO;2

Vignon, E., Alexander, S. P., DeMott, P. J., Sotiropoulou, G., Gerber, F., Hill, T. C. J., et al. (2021). Challenging and improving the simulation of mid-level mixed-phase clouds over the high-latitude southern ocean. *Journal of Geophysical Research: Atmospheres*, *126*(7), e2020JD033490. https://doi.org/10.1029/2020JD033490

Vionnet, V., Martin, E., Masson, V., Guyomarc'h, G., Naaim Bouvet, F., Prokop, A., et al. (2014). Simulation of wind-induced snow transport and sublimation in alpine terrain using a fully coupled snowpack/atmosphere model. *The Cryosphere*, *8*(2), 395–415. https://doi.org/10.5194/tc-8-395-2014

Wang, Y., Ding, M., van Wessem, J. M., Schlosser, E., Altnau, S., van den Broeke, M. R., et al. (2016). A comparison of Antarctic ice sheet surface mass balance from atmospheric climate models and in situ observations. *Journal of Climate*, *29*(14), 5317–5337. https://doi.org/10.1175/JCLI-D-15-0642.1

Wever, N., Würzer, S., Fierz, C., & Lehning, M. (2016). Simulating ice layer formation under the presence of preferential flow in layered snowpacks. *The Cryosphere*, *10*(6), 2731–2744. https://doi.org/10.5194/tc-10-2731-2016

Winker, D. M., Vaughan, M. A., Omar, A., Hu, Y., Powell, K. A., Liu, Z. Y., et al. (2009). Overview of the CALIPSO mission and CALIOP data processing algorithms. *Journal of Atmospheric and Oceanic Technology*, *26*(11), 2310–2323. https://doi.org/10.1175/2009jtecha1281.1

WRF. (2023). WRF code version 4.2 [Software]. WRF. Retrieved from https://github.com/wrf-model/WRF/releases/tag/v4.2

Yang, Z.-L., Niu, G.-Y., Mitchell, K. E., Chen, F., Ek, M. B., Barlage, M., et al. (2011). The community Noah land surface model with multiparameterization options (Noah-MP): 2. Evaluation over global river basins. *Journal of Geophysical Research*, *116*(D12), D12110. https://doi.org/10.1029/2010JD015140